ATLAS NOTE

ATLAS-CONF-2010-088

August 21, 2010

Search for new physics in multi-body final states at high invariant masses with ATLAS

The ATLAS Collaboration

Abstract

Preliminary results of a search for new physics in multi-body final states in proton-proton collisions at a centre-of-mass energy of $\sqrt{s} = 7$ TeV are presented. The data were collected in 2010 with the ATLAS detector at the LHC and correspond to an integrated luminosity of $(295 \pm 32)\,\mathrm{nb}^{-1}$. We observe 193 events with at least three objects in the final state and an invariant mass above 800 GeV and $\sum p_{\mathrm{T}} > 700$ GeV, in agreement with the Standard Model prediction of $254 \pm 18 \pm 84$. An upper limit of 0.34 nb, at the 95% confidence level, is determined for the production cross section times acceptance for new physics models that result in these final states. The result is of interest for models of low-scale gravity and weakly-coupled string theory.

1 Introduction

The search for new physics phenomena beyond the Standard Model is a major goal of the ATLAS detector. A broad range of models have been developed over the past decades which address questions as yet unanswered in the Standard Model. One of the key issues is the apparent weakness of gravity compared to the other known fundamental forces. In other words, why is the Planck scale, $M_{\rm Pl} \sim 10^{19}$ GeV, about sixteen orders of magnitude higher than the electroweak scale? A possible solution to this hierarchy problem is offered by theories with a new gravity scale of about 1 TeV [1–8]. One popular idea postulates a number of extra spatial dimensions. The observed weakness of gravity is then due to the gravitational field propagating into the higher-dimensional space (bulk), while the Standard Model fields are confined to our familiar three-dimensional space (brane) or localised in limited regions of the bulk. In these models, the fundamental scale of gravity, M_D [9], can be in the TeV range, while the Planck scale is an effective scale seen in a three-dimensional world. The relationship between the two scales is model-dependent.

Some low-scale gravity models predict the production of gravitational states close to the new mass scale and continuum production of non-perturbative states above it. For example, the production of black holes [10–12], string balls [6,13], and p-branes [14,15] could occur. In this paper, we search for evidence of such new states. Since the production and decay occurs in the strong-gravity regime and we lack a UV-complete theory of quantum gravity, there are few robust theoretical predictions of their production and decay properties. Well above the gravitational scale, it is anticipated that the semi-classical description of Hawking evaporation [16] and black hole thermodynamics [17–19] will be applicable.

We refer to previous experimental limits [9], to determine the mass scale at which to conduct our search. These limits permit the fundamental scale of gravity to be below 1 TeV, depending on the model assumptions. The lower limit from collider experiments on the fundamental scale M_D in ADD models [1–3] decreases with increasing number of extra dimensions. For six extra dimensions it is 940 GeV [20], while for greater than six extra dimensions it is about 800 GeV [21]. We search in the invariant mass spectrum above 800 GeV.

We rely on a few basic assumptions for the behaviour of final states arising from gravity in the quantum regime. We expect deviations from the Standard Model predictions, in the invariant mass distribution of several high-$p_{\rm T}$ objects. It is assumed that gravity couples only to the energy-momentum content of matter and thus the decays of strong-gravitational objects are approximately democratic to all degrees of freedom in the Standard Model. Therefore, we include the detector signatures from the low-mass fundamental objects of the Standard Model in our search: electrons, photons, muons, and jets. In the semi-classical regime, we expect the decay to involve a large number of high-energy particles. We make no requirement on the particle types or their number other than the requirement that their total number is greater than two. We attempt to keep the search as general as possible, and be guided only by kinematics in choosing our requirements for reducing the backgrounds. This is the first search of this type.

2 ATLAS detector

The ATLAS detector is a multipurpose apparatus with a nominally forward-backward symmetric cylindrical geometry and near 4π coverage in solid angle [22]. The overall layout of the detector is driven by its four magnet systems: a thin superconducting solenoid surrounding an inner tracking cavity and three large superconducting toroids (one barrel and two end caps) surrounding the calorimeters with an eightfold azimuthal symmetry. The calorimeters, which are surrounded by an extensive muon system,

are of particular importance to this analysis. In the pseudo-rapidity region[1] $|\eta| < 3.2$, high-granularity liquid-argon (LAr) electromagnetic sampling calorimeters with very good energy resolution are used. A scintillator-tile calorimeter provides hadronic coverage in the range $|\eta| < 1.7$ and comprises a large central barrel and two smaller extended barrel cylinders, one on each side. The end-cap and forward regions, spanning $1.5 < |\eta| < 4.9$, are again instrumented with LAr calorimetry for both electromagnetic and hadronic energy measurements.

3 Data sample, event selection, and object reconstruction

A sample of events was collected corresponding to $295\,\text{nb}^{-1}$ of proton-proton collisions. A single un-prescaled lowest-level (L1) hardware-based calorimeter jet trigger with a nominal energy threshold of 15 GeV is required. These events are required to have at least five tracks from a reconstructed primary vertex with a z-position within 15 cm of the LHC beam position. This requirement suppresses beam-induced backgrounds and cosmic-ray events. 1% of events are removed by the vertex requirement. Additional quality criteria are applied to the events to ensure that jets are not produced by single noisy calorimeter cells or problematic detector regions [23].

Jets are reconstructed using the infrared- and collinear-safe anti-k_{T} jet clustering algorithm [24] with a radius parameter of 0.4 using energy depositions in topological calorimeter clusters as input [25]. An average correction, determined as a function of jet transverse momentum and pseudo-rapidity, and extracted by numerical inversion from Monte Carlo simulation, is applied to the measured jets to obtain an improved transverse momentum measurement [26]. For object selection, jets with transverse momentum $p_{\text{T}} > 40\,\text{GeV}$ and pseudo-rapidity $|\eta| < 2.8$ are included.

Electron and photon reconstruction is based on clusters of a fixed size in $\eta \times \phi$ in the electromagnetic calorimeter. Electrons are reconstructed from the clusters if there is a suitable match with a track of transverse momentum above 0.5 GeV. Photons are reconstructed from the clusters if there is no reconstructed track matched to the cluster (unconverted photon candidates) or if there is a reconstructed conversion vertex matched to the cluster (converted photon candidates).

Electromagnetic objects are selected as follows: electrons and photons with transverse momentum $p_{\text{T}} > 20\,\text{GeV}$, and pseudo-rapidity $|\eta| < 2.47$ for electrons and $|\eta| < 2.37$ for photons. Electrons and photons in the transition regions of the calorimeter $1.37 < |\eta| < 1.52$ are not identified as electrons and photons, but could be included as jets if they are also identified by the jet reconstruction algorithm.

A combined muon reconstruction algorithm is used in this analysis. This associates a standalone muon spectrometer track with an inner detector track using a χ^2 consistency criterion, based on the difference between the two sets of track parameters weighted by their combined covariance matrix. For the object selection, muons with transverse momentum $p_{\text{T}} > 20\,\text{GeV}$ and pseudo-rapidity $|\eta| < 2.0$ are included.

The missing transverse energy of the event, $E_{\text{T}}^{\text{miss}}$, is used in the calculation of the invariant mass of the event. It is reconstructed using calorimeter cells belonging to clusters in the pseudo-rapidity range $|\eta| < 4.8$. This cell selection provides efficient noise suppression [27]. The energy of muon candidates is subtracted in the calculation.

The identification of detector signatures as final-state objects can be ambiguous. The same detector hits can be reconstructed as two different objects with a small separation in ΔR, where $\Delta R \equiv \sqrt{\Delta\eta^2 + \Delta\phi^2}$, and $\Delta\eta$ ($\Delta\phi$) are the differences between the reconstructed pseudo-rapidities (azimuthal

[1] The ATLAS reference system is a Cartesian right-handed coordinate system, with a nominal collision point at the origin. The anticlockwise beam direction defines the positive z-axis, while the positive x-axis is defined as pointing from the collision point to the centre of the LHC ring and the positive y-axis points upwards. The azimuthal angle ϕ is measured around the beam axis in the transverse (xy)-plane, and the polar angle θ is measured with respect to the z-axis. The pseudo-rapidity is defined as $\eta = -\ln(\tan(\theta/2))$.

angles) of the two objects. In such cases, if $\Delta R < 0.1$ between an electron and a photon, or $\Delta R < 0.2$ between a jet, and either an electron or a photon, the ambiguity is resolved by selecting electrons, photons, and jets, in that order of priority. Muons are not included in this procedure, as muons produced close to jets are unlikely to have their energy included in the jet energy. We do not attempt further object identifications, for example to tag taus or heavy-flavour decays, or the reconstruction of heavier states such as W-bosons, Z-bosons, and top quarks. Not reconstructing these objects has no impact on the invariant mass of the event.

4 Standard Model Backgrounds

The dominant Standard Model background for this search is QCD jet production [28]. The predictions for this process are subject to uncertainties. However, the analysis method we use is designed to avoid many of the uncertainties in QCD predictions by extrapolating from a nearby region where no new physics is present. The analysis is sensitive to uncertainties in QCD effects, such as higher-order QCD radiation, showering, and hadronisation. To estimate the effect of hard radiation, two event generators, PYTHIA 6.421 [29] and ALPGEN 2.06 [30], are used. PYTHIA produces two hard jets using leading-order (LO) matrix elements. High-multiplicity final states appear as a result of QCD shower processes. In contrast, ALPGEN produces up to six hard jets in the final state using leading order QCD matrix element calculations for multi-parton final states, and Mangano (MLM) matching to combine them with parton shower models. ALPGEN is combined with JIMMY 4.3 [31] for the underlying event simulation and HERWIG 6.510 [32] for the parton shower simulation and hadronisation. For comparison, we also use the LO implementation of the HERWIG and HERWIG++ 2.4.2 [33] Monte-Carlo event generators. These two generators also use the parton-shower approach to generate initial- and final-state QCD radiation, including colour coherence effects.

Another background source is $t\bar{t}$ production, which is generated using MC@NLO [34]. In addition, ALPGEN is used to simulate potential contributions from W-boson plus jets Standard Model processes. Previous studies have shown [28] that other backgrounds are much smaller and can be neglected in this analysis.

The ATLAS MC09 PYTHIA tune is used as baseline [35]. To study the effects of the uncertainty in describing soft QCD, we use data sets from two alternative tunes of PYTHIA: an alternative fragmentation tune and a different underlying-event model [36]. For the alternative underlying event, we use Perugia0 from the set of Perugia tunes [37]. This is a set of tunes using $p_{\perp}$-ordered showers with PYTHIA version 6.4 and CTEQ5L parton distribution functions (PDFs).

Different parton distribution functions are used with these generators. The baseline PYTHIA, HERWIG, and HERWIG++ event samples are generated using MRST 2007 LO* [38], a PDF set specifically tuned to provide a cross section description for a number of Standard Model processes, which are close to the next-to-leading-order (NLO) prediction, by combining it with leading-order matrix elements. For ALPGEN simulations, a leading-order PDF set, CTEQ 6 L1 [39], is used. CTEQ 6.6 was used for the MC@NLO $t\bar{t}$ samples.

The detector response for all the generated Monte Carlo events is simulated by passing them through a detailed simulation of the ATLAS detector based on the GEANT4 program [40,41]. These detector simulated events are then reconstructed, selected, and analysed identically to the data.

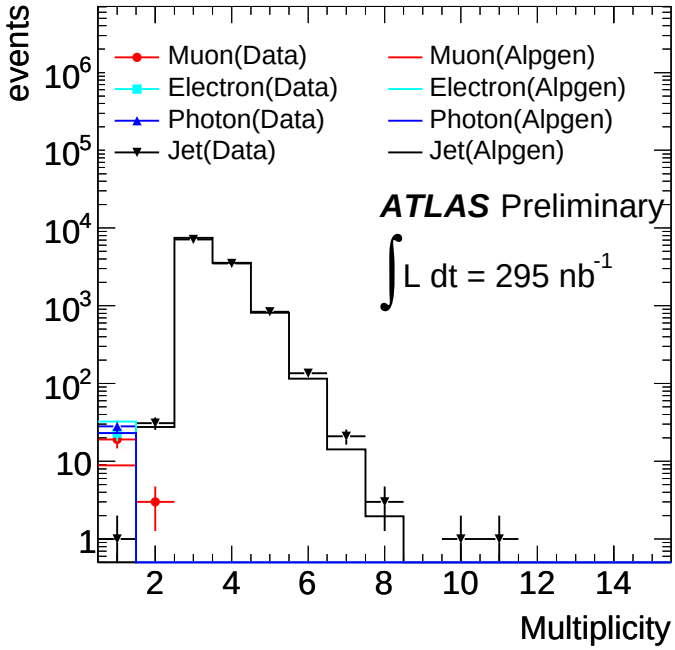

Figure 1: Object multiplicity for events after a requirement of $\sum p_{\mathrm{T}} > 300\,\mathrm{GeV}$. The markers represent the data and the histograms the background predictions obtained using ALPGEN simulations. The jet, electron, photon, and muon distributions are shown in black, cyan, blue, and red respectively.

5 Analysis procedure

5.1 Signal and control regions

We use an analysis strategy that strongly suppresses Standard Model backgrounds, while preserving a high efficiency for a possible high-mass multi-particle final state. We require at least three objects selected according to the criteria in section 3. This reduces low-p_{T} and two-body scattering processes, while having little effect on a potential high invariant mass signal. After the basic event selection, 92527 events with three or more objects remain.

The scalar sum of the transverse momentum of all reconstructed objects in an event,

$$\sum p_{\mathrm{T}} \equiv \sum_{i=\mathrm{objects}} p_{\mathrm{T}i}\,, \tag{1}$$

is a variable that is strongly correlated to the invariant mass of the event for central production processes. It is a useful variable for reducing the QCD $2 \to 2$ scattering amplitudes characterised by a strong forward peak in the differential cross section, as it selects more centrally produced objects, reducing our exposure to jet systematics from the forward region. Figure 1 shows the multiplicities of each type of object in events after a requirement of $\sum p_{\mathrm{T}} > 300\,\mathrm{GeV}$ for data and the simulated background. The events are dominated by jets, with a tiny admixture of electrons, photons, and muons. Most common are three jet events, with those containing four and five jets also significant. Requiring $\sum p_{\mathrm{T}} > 300\,\mathrm{GeV}$, selects 11664 events with more than two objects. On visual inspection, the two events in the high-multiplicity tail were found to be non-collision background events. Further work will be undertaken to study and reduce this potential background. These two events are removed by the requirements we impose on the signal events.

We search for an excess of events in the high invariant mass of the final state calculated from all objects in the event using the formula

$$M_{\text{inv}} = \sqrt{p^2} \quad \text{and} \quad p = \sum_{i=\text{objects}} p_i + (E_{\text{T}}^{\text{miss}}, E_{\text{T}x}^{\text{miss}}, E_{\text{T}y}^{\text{miss}}, 0)\,, \tag{2}$$

where p_i is the reconstructed four-momenta of the objects and $E_{\text{T}}^{\text{miss}}$ is the missing transverse energy in the event, and $E_{\text{T}x}^{\text{miss}}$ and $E_{\text{T}y}^{\text{miss}}$ are the x- and y-components, respectively. A good mass reconstruction is obtained by summing momenta of the reconstructed objects above certain thresholds and including the missing transverse energy. When summing reconstructed objects, it is important to include all identified objects, and to avoid double counting the energy from overlapping objects, as described in section 3.

Due to finite mass resolution effects and the steeply falling parton distribution functions with increasing parton centre-of-mass energy, there is considerable migration of events from their true mass values to the reconstructed ones. Our final result is based on counting events above the reconstructed mass threshold of 800 GeV after a requirement of $\sum p_{\text{T}} > 700$ GeV, and is presented as a cross section times acceptance.

Since the cross sections for Monte Carlo simulations can only approximate the true multi-jet cross section, the Monte Carlo samples are normalised to the number of observed events in a control region, where no new physics effects are expected. The method we use is designed to reduce the uncertainties in QCD predictions by extrapolating from a nearby control region, and hence, we only rely on the simulation of the shape of the differential cross section in mass.

A grid of possible control regions is studied. A minimum $\sum p_{\text{T}}$ requirement ranging from 200 GeV to 400 GeV, and minimum invariant mass of 200 GeV to 500 GeV, with each being varied in 100 GeV steps are examined. The maximum invariant mass of the chosen control region is 800 GeV in all cases. A control region consisting of an invariant mass range between 300 GeV and 800 GeV, and a mild $\sum p_{\text{T}}$ requirement of 300 GeV is chosen. This region provides adequate Monte Carlo statistics in a similar kinematic regime to the signal region. In the case of ALPGEN, using an adjacent control region changes the predicted number of events in the signal region by less than 2.4%. The PYTHIA, HERWIG, and HERWIG++ predictions vary more dramatically across the possible control regions resulting in changes in the predicted number of events in the signal region by up to about 10%, 20%, and 20%, respectively. We take 10% as a systematic uncertainty on the estimated background due to our choice of control region. In the control region, there are 9215 data events, containing a total of 31454 jets, 17 electrons, 26 photons, and 24 muons.

Figure 2 shows the $\sum p_{\text{T}}$ distribution for data and the simulated background after requiring at least three objects in the event. The ALPGEN predictions have been normalised to data in the region $\sum p_{\text{T}} > 300$ GeV and $300 < M_{\text{inv}} < 800$ GeV.

The normalisation of the background is performed by scaling the ALPGEN prediction for the cross section by a factor of 1.15 and the PYTHIA predictions by a factor of 0.64, respectively. Figure 3 shows the object transverse momentum distribution and missing transverse energy distribution for events in the control region compared to ALPGEN, when normalised to data in the control region. A comparison of the invariant mass from ALPGEN, PYTHIA, and data for the control and signal regions are displayed in Figure 4.

The signal region, $\sum p_{\text{T}} > 700$ GeV and $M_{\text{inv}} > 800$ GeV, contains 193 events. These events contain 769 jets, and no electrons, photons, or muons. After rescaling using the events in the control region, ALPGEN predicts 254 ± 18 events, while PYTHIA predicts 174 ± 11 events, where the uncertainties are due to the limited statistics of the Monte Carlo simulations.

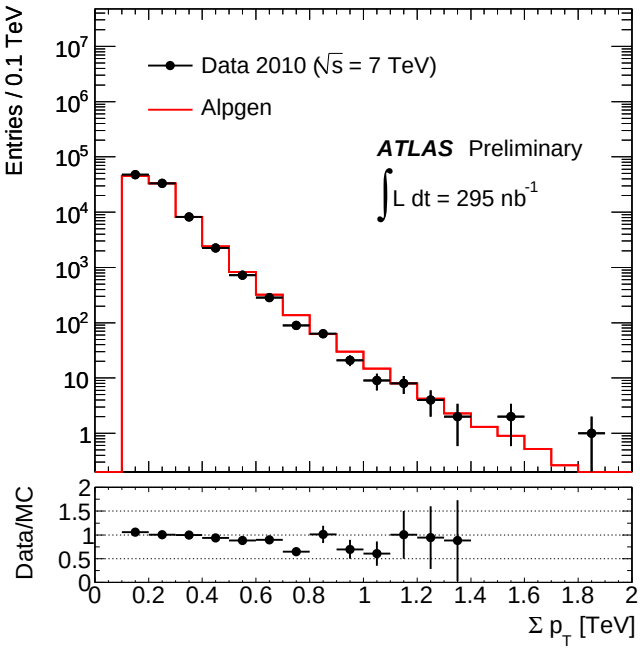

Figure 2: Distribution of the scalar sum of the transverse momenta of all objects in the event, after requiring at least three objects in the event. The solid black dots represent the data and the red histogram the background prediction obtained using ALPGEN simulation. The lower panel shows the ratio of the data to the ALPGEN predictions (solid black dots). The simulated background is scaled to the number of data events in a control region $\sum p_{\mathrm{T}} > 300\,\mathrm{GeV}$ and $300\ \mathrm{GeV} < M_{\mathrm{inv}} < 800\ \mathrm{GeV}$.

5.2 Background Uncertainties

The background estimation is subject to three major uncertainties due to: QCD radiation and fragmentation effects; parton distribution functions; and jet-energy scale and jet-energy resolution uncertainties.

In order to estimate the uncertainty due to QCD effects, the predictions of ALPGEN, PYTHIA, HERWIG, and HERWIG++ were compared with each other. We studied our sensitivity to some of the parameters used in QCD simulations, by using an alternative fragmentation tune and different underlying-event model. The different fragmentation tune gives a 0.1% increase in the number of events in the signal region. The Perugia0 tune which contains a different underlying event model, results in a 10% increase in the number of events in the signal region.

For the background estimate, the ALPGEN prediction is used, as it better represents multiple hard jets and is more stable with respect to changes in the control region. ALPGEN and PYTHIA bracket the range of background predictions in the signal region, include the HERWIG and HERWIG++ predictions, and PYTHIA predictions for two alternative tunes. The difference in the predictions between ALPGEN and PYTHIA, re-weighted to the CTEQ6L1 PDFs used by ALPGEN, is taken as a systematic uncertainty on the background due to QCD effects. Our best estimate of the background is $254 \pm 18 \pm 67$ events, where the former uncertainty is the statistical uncertainty, and the latter the systematic uncertainty due to QCD modelling.

The uncertainty due to PDFs is estimated as follows. The events generated with ALPGEN are re-weighted according to the Bjorken-x values of the interacting partons from the production process and its scale Q^2, as given by CTEQ6L1 to the CTEQ6.6 central next-to-leading order set. The full set of error eigenvectors of CTEQ6.6 are combined following the recipe of Ref. [42] to estimate the spread of next-

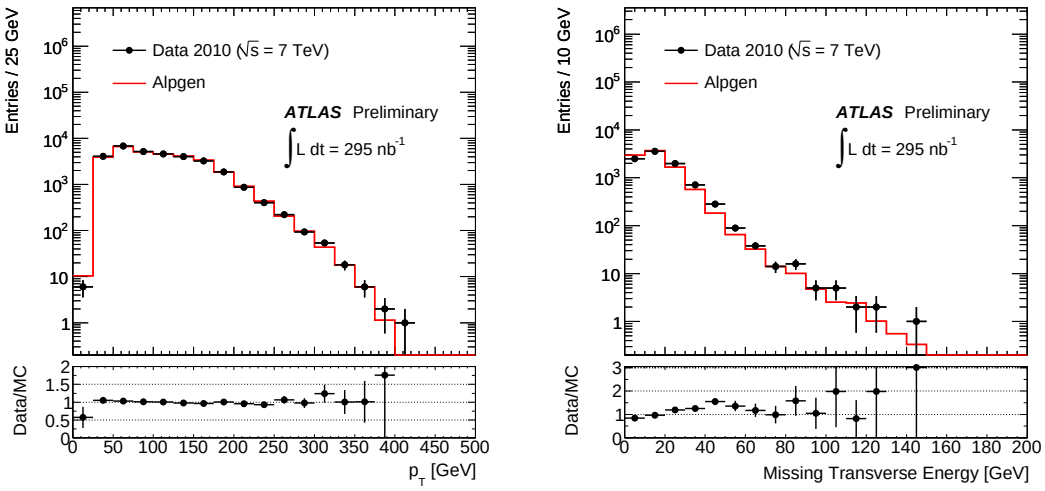

Figure 3: Transverse momentum of all objects (left) and missing transverse energy in events (right) for events in the control region $\sum p_{\mathrm{T}} > 300$ GeV and 300 GeV $< M_{\mathrm{inv}} <$ 800 GeV. The solid black dots are the data, while the red histograms are the background predictions using ALPGEN normalised to data in the control region. The lower panels show the ratio of the data to the ALPGEN predictions (solid black dots).

to-leading order predictions, giving an upper and lower uncertainty on the central CTEQ 6.6 distribution. Then each of these three distributions are normalised to the data in the control region of $\sum p_{\mathrm{T}} > 300$ GeV and $300 < M_{\mathrm{inv}} < 800$ GeV, and the resulting expectation in the signal region determined. Compared to the number of events predicted using CTEQ 6L1, CTEQ 6.6 predicts 1% more events for its central set, and variations of $+7\%$ and -5% from the central set due to the PDF error sets. The differences due to the error sets are added in quadrature to the other systematic uncertainties and used as an uncertainty in our estimate of the background due to PDF uncertainties. In addition, the ALPGEN events are re-weighted to the MRST 2007 LO* PDF set that is used by PYTHIA. The predicted number of ALPGEN events decreases by 12% after the re-weighting. This difference is used as an additional uncertainty in our estimate of the background due to different model assumptions among the different PDF groups.

The uncertainty due to the jet-energy scale is estimated using a rapidity and transverse-momentum dependent rescaling function [43–45]. This depends upon the number of vertices reconstructed (with 5 or more tracks). For each Monte Carlo event, a number of vertices was selected according to the distribution from data and the corresponding jet energy scale uncertainty used. For the case of no additional vertex, the overall uncertainty of the jet-energy scale is below 9% over the entire range of p_{T} and η considered, and below 7% for central jets with $p_{\mathrm{T}} > 60$ GeV. The effect of the jet-energy scale uncertainty on the predicted background is $+6\%$ and -7%. Concordant numbers are obtained for the ALPGEN and PYTHIA samples.

Since the topology of the analysed events differs from those used to obtain the energy uncertainty function, an additional uncertainty due to the different response between quark and gluon jets is added linearly to all the jets. Including this additional uncertainty changes the predicted background in total by $+7\%$ and -8%.

An additional uncertainty due to jets close to each other is added linearly to the jet-energy uncertainty. For those jets with another jet within $\Delta R < 1$, this additional correction is applied. The correction is independent of p_{T} and η. We take the size of the response correction (4%) as the systematic uncertainty due to close-by soft jets. Including this additional uncertainty, changes the predicted background by

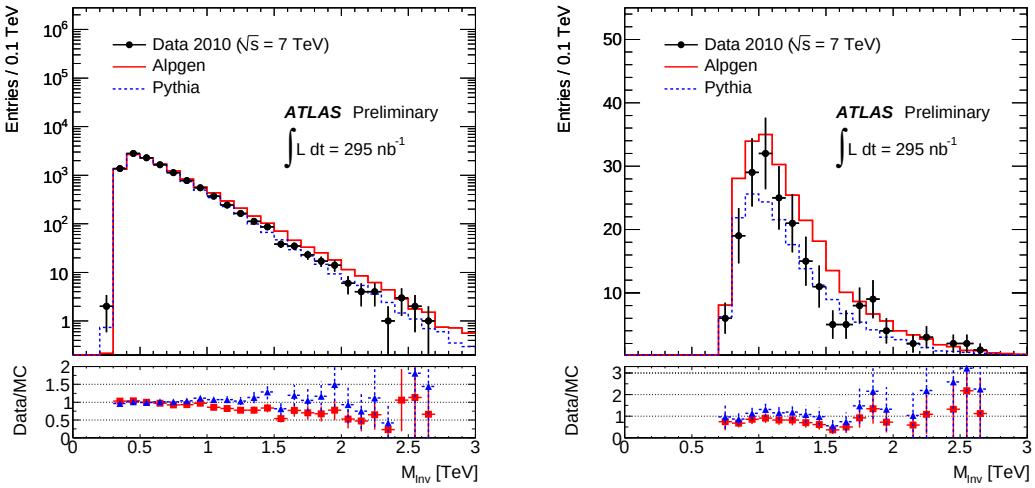

Figure 4: Invariant mass distribution for $\sum p_{\mathrm{T}} > 300\,\mathrm{GeV}$ (left) and $\sum p_{\mathrm{T}} > 700\,\mathrm{GeV}$ (right), after normalising the background to data in the control region. The solid black dots are the data, while the red and blue histograms are the background predictions obtained using ALPGEN and PYTHIA, respectively. The lower panels show the ratio of the data to the ALPGEN predictions (solid red squares) and the PYTHIA predictions (solid blue triangles).

$\pm 11\%$.

The event pile-up, where more than one proton-proton interaction occur at the same bunch-crossing, introduces additional uncertainties. Fewer than 0.2% of the events in the control region have a jet from a second vertex, so we expect fewer than one event in the signal region. Pile-up can also effect the uncertainty of the jet energy scale. Studies of events with multiple reconstructed primary vertices show that jet energies may acquire an additional energy depending on jet pseudo-rapidity η and number of additional vertices. The average contribution is about 0.5 GeV per each additional primary vertex for $|\eta| < 1.9$, and about 2 GeV for larger $|\eta|$. The effect of pile-up was evaluated by subtracting these average contributions from each jet in the data. The effect on the control and signal region is -3% and -4%, respectively .

The propagation of the jet energy scale uncertainty to $E_{\mathrm{T}}^{\mathrm{miss}}$, used in the calculation of the invariant mass, holds an additional uncertainty. The jet energy scale uncertainty is propagated to $E_{\mathrm{T}}^{\mathrm{miss}}$ by subtracting the original jets and adding back the modified ones. The difference between the predicted number of events in the signal region after this procedure is less than 0.5% compared with that calculated with no change to $E_{\mathrm{T}}^{\mathrm{miss}}$. This difference is included as an additional uncertainty. A further $E_{\mathrm{T}}^{\mathrm{miss}}$ uncertainty due to the energy measured outside of reconstructed jets is negligible, since the total energy in the calorimeter is dominated by jets.

There is a possible uncertainty in the number of estimated background events due to the uncertainty in the jet-energy resolution. To estimate the effect of jet-energy resolution uncertainty, we use the bisector raw resolution approach [46]. The jet-energy resolution is 14% [46] for jets with p_{T} values between 20 GeV and 80 GeV, which is conservative for more highly energetic jets. We add additional Gaussian smearing to the jet transverse momentum, and repeat the analysis to study the change in the number of predicted background events. The number of predicted signal events increases by 0.6%. We assigned a 0.6% additional systematic uncertainty to the estimated number of background events due to the jet-energy resolution.

Additional uncertainties of the background estimation arise from other Standard Model contributions

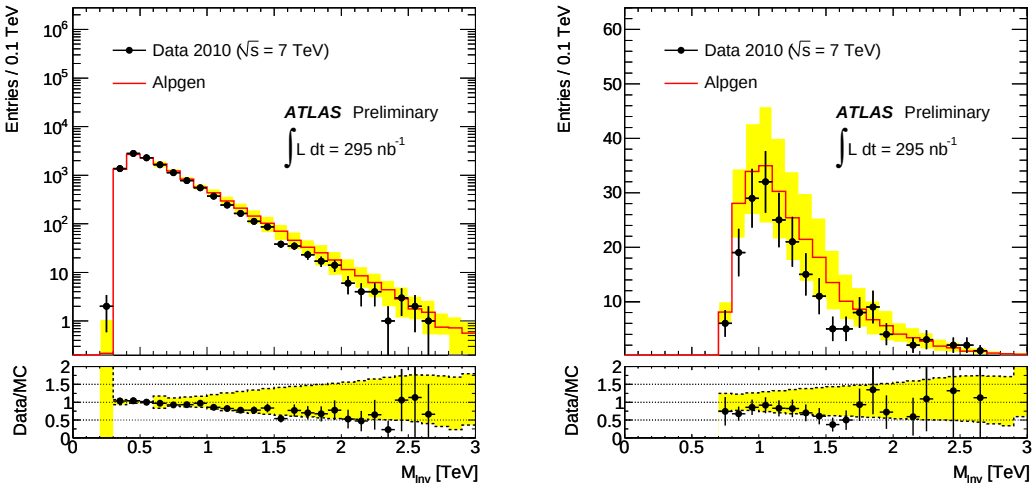

Figure 5: Invariant mass distributions for (left) $\sum p_{\mathrm{T}} > 300\,\mathrm{GeV}$ and (right) $\sum p_{\mathrm{T}} > 700\,\mathrm{GeV}$. The solid black dots are the data and the red histograms are the background predictions obtained using ALPGEN simulation. The background prediction is scaled to the number of data events in a control region $\sum p_{\mathrm{T}} > 300\,\mathrm{GeV}$ and $300 < M_{\mathrm{inv}} < 800\,\mathrm{GeV}$, after requiring at least three objects in the event. The error band on the background is the total uncertainty: statistical (negligible) and all systematic uncertainties added in quadrature. The lower panels show the ratio of the data to the background predictions (solid black dots) and the same error band on the background (yellow).

to the background. These contributions are anticipated to be negligible, with the highest contribution estimated to be from top-quark production, W-boson plus jets, and Z-boson plus jets [28]. Their contribution of 1.5 events in the signal region is small, and is treated as an additional systematic uncertainty on the background determination due to Standard Model processes that we have not explicitly included.

The number of background events, including all uncertainties, is estimated to be $254 \pm 18 \pm 84$, where the first uncertainty is statistical and the second systematic. All uncertainties on the background estimate are added in quadrature to obtain an overall background uncertainty of $\pm 34\%$, including statistical and systematic contributions. Figure 5 shows reconstructed invariant mass distributions for data and simulated background after normalising ALPGEN to the control region. The error band on the simulated background corresponds to the total uncertainty.

6 Experimental results

A summary of all the numerical results can be found in Table 1. After all the event selections, we observe 193 events above an invariant mass of 800 GeV and with $\sum p_{\mathrm{T}} > 700\,\mathrm{GeV}$. The observed number of events is consistent with the estimated background of $254 \pm 18 \pm 84$ events; the first uncertainty is statistical and the second uncertainty is systematic. An 11% systematic uncertainty is assigned to the luminosity value obtained from van der Meer beam scans [47]. Based on these numbers of events and an integrated luminosity of $(295 \pm 32)\,\mathrm{nb}^{-1}$, we calculate an upper limit on the production cross section times acceptance[2]. Using a Bayesian approach and assuming a flat prior p.d.f. for the signal events, we obtain an upper limit of 0.34 nb, at the 95% confidence level. If we subtract the additional contribution due to pile-up from data, we obtain an upper limit of 0.32 nb.

[2]The cross-section limit is calculated as usual, with the assumption of 100% acceptance.

Table 1: Summary of the numerical results. The QCD background systematic is the difference between ALPGEN and PYTHIA, after re-weighting to the same PDF, as described in section 4.

Quantity	Value	Uncertainty	Uncertainty [%]
Data			
Observed events	193		
Luminosity [nb^{-1}]	295	$\pm$32	$\pm$11%
Estimated Background			
ALPGEN	254	$\pm$18	6.9%
PYTHIA	174	$\pm$11	6.2%
Background (statistical)	254	$\pm$18	6.9%
Systematic Uncertainties			
Background (QCD)		$\pm$66.5	26%
PDF (choice)			$\pm$12%
PDF (error set)			$+$6.8%
PDF (error set)			$-$5.2%
Control region			$\pm$10%
Un-simulated backgrounds			$\pm$0.6%
Including e, γ, μ			$\pm$0.2%
Missing transverse energy			$\pm$0.02%
JES			$\pm$11.0%
JES (MET)			$\pm$0.5%
JER			$\pm$0.6%
Systematic uncertainty		$+$84	$+$33%

7 Discussion

For an estimation of detector acceptance for high invariant-mass states in low-scale gravity models, we generated Monte Carlo event samples using the event generators CHARYBDIS 2 [48] and BLACKMAX 2 [49,50].

In this analysis, we search for multi-body final states with invariant mass above 800 GeV. Since the experimental limit on the Planck scale in ADD models is 800 GeV, or higher depending on the model parameters, the validity of the physics models used in the above generators is questionable for masses close to the Planck scale. However, the above event generators provide a means of simulating the kinematic characteristics of high invariant mass multi-object final states. Several different samples are generated with a range of decay topologies.

We generated three black hole samples using CHARYBDIS with fixed decay multiplicities of three, four, and five primary particles. In addition, we generated a BLACKMAX event sample using its final burst model [49,50]. All the samples are produced with an energy threshold equal to the Planck scale of 800 GeV and six extra dimensions. The samples are produced with CTEQ 6.6 PDF [51]. These are interfaced to PYTHIA for the simulation of QCD effects including parton showers, underlying event, and hadronisation. Subsequently, all the samples are passed through the simulation of the detector response and the event reconstruction.

Using the BLACKMAX sample, the acceptance after all selection requirements and for a reconstructed invariant mass above 800 GeV is (58 ± 2)%, where the uncertainty is due to the limited statistics of the Monte Carlo simulated sample. The three CHARYBDIS samples give similar acceptances to BLACKMAX to within 4%. In spite of good agreement between the simulated signal acceptances, the systematic

uncertainty in the acceptance is expected to be large due to the lack of a well established physics model in the mass region near the gravity scale. Using the BlackMax acceptance value as an illustration, the upper limit on the production cross section for high invariant mass events above 800 GeV is 0.6 nb.

In the most optimistic calculation, the maximum black hole cross-section, can be $\mathcal{O}(100)$ nb [48,49], considering the geometric cross section at a mass threshold of 800 GeV. Our illustrative upper limit is well below this value.

This search is less sensitive to cases with large missing energy produced by scenarios involving black hole remnants, significant gravitational radiation in the production process or graviton emission in the decay.

Further searches may produce more restrictive limits by making more specific model assumptions. For example, the Standard Model background can be strongly suppressed by a requirement of at least one electron or muon in the final state [28]. Assuming an approximately democratic decay of strong-gravitational objects, this would provide a high efficiency for the signal. The transverse momentum requirements will need to be optimised to reduce small angle QCD scattering when the search is performed at higher invariant masses.

8 Summary

Preliminary results of a first search for exotic multi-body final states at high invariant masses are presented. The analysis used proton–proton collisions at a centre-of-mass energy of 7 TeV recorded with the ATLAS detector at the LHC. The data were collected in 2010 and correspond to an integrated luminosity of $295\,\text{nb}^{-1}$. We observe 193 events with at least three particles in the final state and an invariant mass above 800 GeV and $\sum p_{\text{T}} > 700$ GeV in agreement with the Standard Model prediction of $254 \pm 18 \pm 84$. An upper limit of 0.34 nb, at the 95% confidence level, is determined for the production cross section times acceptance for new physics models that result in these final states. The result is of interest for models of low-scale gravity and weakly-coupled string theory.

References

[1] N. Arkani-Hamed, S. Dimopoulos, and G. R. Dvali, *The hierarchy problem and new dimensions at a millimeter*, Phys. Lett. B **429** (1998) 263. arXiv:hep-ph/9803315.

[2] I. Antoniadis, N. Arkani-Hamed, S. Dimopoulos, and G. R. Dvali, *New dimensions at a millimeter to a Fermi and superstrings at a TeV*, Phys. Lett. B **436** (1998) 257. arXiv:hep-ph/9804398.

[3] N. Arkani-Hamed, S. Dimopoulos, and G. R. Dvali, *Phenomenology, astrophysics and cosmology of theories with sub-millimeter dimensions and TeV scale quantum gravity*, Phys. Rev. D **59** (1999) 086004. arXiv:hep-ph/9807344.

[4] L. Randall and R. Sundrum, *A large mass hierarchy from a small extra dimension*, Phys. Rev. Lett. **83** (1999) 3370. arXiv:hep-ph/9905221.

[5] L. Randall and R. Sundrum, *An alternative to compactification*, Phys. Rev. Lett. **83** (1999) 4690. arXiv:hep-th/9906064.

[6] S. Dimopoulos and R. Emparan, *String balls at the LHC and beyond*, Phys. Lett. B **526** (2002) 393. arXiv:hep-ph/0108060.

[7] G. Dvali, *Black holes and large N species solution to the hierarchy problem*, arXiv:0706.2050 [hep-th] (2007) .

[8] G. Dvali and M. Redi, *Black holes bound on the number of species and quantum gravity at the LHC*, Phys. Rev. D **77** (2008) 045027. arXiv:0710.4344 [hep-th].

[9] Particle Data Group Collaboration, C. Amsler et al., *Review of particle physics*, Phys. Lett. B **667** (2008) 1.

[10] T. Banks and W. Fischler, *A model for high energy scattering in quantum gravity*, arXiv:hep-th/9906038 (1999) .

[11] S. B. Giddings and S. D. Thomas, *High energy colliders as black hole factories: The end of short distance physics*, Phys. Rev. D **65** (2002) 056010. arXiv:hep-ph/0106219.

[12] S. Dimopoulos and G. L. Landsberg, *Black holes at the LHC*, Phys. Rev. Lett. **87** (2001) 161602. arXiv:hep-ph/0106295.

[13] D. M. Gingrich and K. Martell, *Study of highly-excited string states at the Large Hadron Collider*, Phys. Rev. D **78** (2008) 115009. arXiv:0808.2512 [hep-ph].

[14] K. Cheung and C.-H. Chou, *p-brane production in fat brane or universal extra dimension scenario*, Phys. Rev. D **66** (2002) 036008. arXiv:hep-ph/0205284.

[15] E.-J. Ahn, M. Cavaglià, and A. V. Olinto, *Brane factories*, Phys. Lett. B **551** (2003) 1. arXiv:hep-th/0201042.

[16] S. Hawking, *Particle creation by black holes*, Commun. math. Phys. (1975) .

[17] J. D. Bekenstein, *Black holes and entropy*, Phys. Rev. D **7** (1973) 2333.

[18] J. D. Bekenstein, *Generalized second law of thermodynamics in black-hole physics*, Phys. Rev. D **9** (1974) 3292.

[19] S. W. Hawking, *Black holes and thermodynamics*, Phys. Rev. D **13** (1976) 191.

[20] CDF Collaboration, T. Aaltonen et al., *Search for large extra dimensions in final states containing one photon or jet and large missing transverse energy produced in $p\bar{p}$ collisions at $\sqrt{s} = 1.96\,TeV$*, Phys. Rev. Lett. **101** (2008) 181602. arXiv:0807.3132 [hep-ex].

[21] D0 Collaboration, V. M. Abazov et al., *Search for large extra dimensions via single photon plus missing energy final states at $\sqrt{s} = 1.96\,TeV$*, Phys. Rev. Lett. **101** (2008) 011601. arXiv:0803.2137 [hep-ex].

[22] ATLAS Collaboration, G. Aad et al., *The ATLAS experiment at the CERN Large Hadron Collider*, JINST **3** (2008) S08003.

[23] ATLAS Collaboration, *Data-quality requirements and event cleaning for jets and missing transverse energy reconstruction with the ATLAS detector in proton-proton collisions at a center-of-mass energy of $\sqrt{s} = 7\,TeV$*, ATLAS-CONF-2010-038 (2010) .

[24] M. Cacciari, G. P. Salam, and G. Soyez, *The anti-k_T jet clustering algorithm*, JHEP **04** (2008) 063. arXiv:0802.1189 [physics.ins-det].

[25] W. Lampl et al., *Calorimeter clustering algorithms: Description and performance*, ATL-LARG-PUB-2008-002 (2008) .

[26] ATLAS Collaboration, *Observation of energetic jets in pp collisions at $\sqrt{s} = 7$ TeV using the ATLAS experiment at the LHC*, ATLAS-CONF-2010-043 (2010) .

[27] ATLAS Collaboration, G. Aad et al., *Readiness of the ATLAS Liquid Argon Calorimeter for LHC Collisions*, arXiv:0912.2642 [physics.ins-det] (2009) .

[28] ATLAS Collaboration, *Expected performance of the ATLAS experiment: detector, trigger and physics*, arXiv:0901.0512 [hep-ex] (2009) .

[29] T. Sjöstrand, S. Mrenna, and P. Skands, *PYTHIA 6.4 physics and manual*, JHEP **0605** (2006) 026. arXiv:hep-ph/0603175.

[30] M. L. Mangano, M. Moretti, F. Piccinini, R. Pittau, and A. Polosa, *ALPGEN, a generator for hard multiparton processes in hadronic collisions*, JHEP **0307** (2003) 001. arXiv:hep-ph/0206293.

[31] J. M. Butterworth, J. R. Forshaw, and M. H. Seymour, *Multiparton interactions in photoproduction at HERA*, Z. Phys. C **72** (1996) 637. arXiv:hep-ph/9601371.

[32] G. Corcella et al., *HERWIG 6: An event generator for hadron emission reactions with interfering gluons*, JHEP **0101** (2001) 010. arXiv:hep-ph/0011363.

[33] M. Bahr et al., *HERWIG++ Physics and Manual*, Eur. PHys. J. **C58** (2008) 639. arXiv:0803.0883 [hep-ph].

[34] S. Frixione and B. R. Webber, *Matching NLO QCD computations and parton shower simulations*, JHEP **06** (2002) 029. arXiv:hep-ph/0204244.

[35] ATLAS Collaboration, *The ATLAS Monte Carlo tunes for MC09*, ATL-PHYS-PUB-2010-002 (2010) .

[36] A. Buckley, H. Hoeth, H. Lacker, H. Schulz, and J. E. von Seggem, *Systematic event generation tuning for the LHC*, Eur. Phys. J. C **65** (2010) 221. arXiv.0907.2973 [hep-ph].

[37] P. Skands, *The "perugia" Tunes*, arXiv:0905.3418 [hep-ph] (2009) .

[38] A. Sherstnev and R. S. Thorne, *Parton distributions for LO generators*, Eur. Phys. J. C **55** (2008) 553. arXiv:0711.2473 [hep-ph].

[39] J. Pumplin et al., *New generation of parton distributions with uncertainties from global QCD analysis*, JHEP **07** (2002) 012. arXiv:hep-ph/0201195.

[40] GEANT4 Collaboration, S. Agostinelli et al., *GEANT4: A simulation toolkit*, Nucl. Instrum. Meth. A **506** (2003) 250.

[41] J. Allison et al., *Geant4 developments and applications*, IEEE Trans. Nucl. Sci. **53** (2006) 270.

[42] A. D. Martin, W. J. Stirling, R. S. Thorne, and G. Watt, *Parton distributions for the LHC*, Eur. Phys. J. **C63** (2009) 189, `arXiv:0901.0002 [hep-ph]`.

[43] ATLAS Collaboration, *Calorimeter response to single isolated hadrons and estimation of the calorimeter jet scale uncertainty*, ATLAS-CONF-2010-052 (2010) .

[44] ATLAS Collaboration, *Jet energy scale and its systematic uncertainty in ATLAS for jets produced in proton-proton collisions at $\sqrt{s} = 7$ TeV*, ATLAS-CONF-2010-056 (2010) .

[45] ATLAS Collaboration, *In-situ pseudo-rapidity inter-calibration to evaluate jet energy scale uncertainty and calorimeter performance in the forward region*, ATLAS-CONF-2010-055 (2010) .

[46] ATLAS Collaboration, *Jet energy resolution and selection efficiency relative to track jets from in-situ techniques with the ATLAS detector using proton-proton collisions at a center of mass energy* $\sqrt{s} = 7$ *TeV*, ATL-CONF-2010-054 (2010) .

[47] ATLAS Collaboration, *Luminosity Determination using the ATLAS Detector*, ATLAS-CONF-2010-060 (2010) .

[48] J. A. Frost et al., *Phenomenology of production and decay of spinning extra-dimensional black holes at hadron colliders*, JHEP **10** (2009) 014. arXiv:0904.0979 [hep-ph].

[49] D.-C. Dai et al., *BlackMax: A black-hole event generator with rotation, recoil, split branes and brane tension*, Phys. Rev. D **77** (2008) 076007. arXiv:0711.3012 [hep-ph].

[50] D.-C. Dai et al., *Manual of BlackMax, a black-hole event generator with rotation, recoil, split branes, and brane tension*, arXiv:0902.3577 [hep-ph] (2009) .

[51] P. M. Nadolsky et al., *Implications of CTEQ global analysis for collider observables*, Phys. Rev. D **78** (2008) 013004. arXiv:0802.0007 [hep-ph].